HHS Public Access

Author manuscript

Cell Rep Phys Sci. Author manuscript; available in PMC 2022 April 13.

Published in final edited form as:

Cell Rep Phys Sci. 2022 March 16; 3(3): . doi:10.1016/j.xcrp.2022.100802.

Slowing magnetic relaxation with open-shell diluents

Ian P. Moseley[1], **Christopher P. Ard**[2], **Joseph A. DiVerdi**[1], **Andrew Ozarowski**[3], **Hua Chen**[2,4], **Joseph M. Zadrozny**[1,5,*]

[1]Department of Chemistry, Colorado State University, Fort Collins, CO 80523, USA

[2]Department of Physics, Colorado State University, Fort Collins, CO 80523, USA

[3]National High Magnetic Field Laboratory, Tallahassee, FL 32310, USA

[4]School of Advanced Materials Discovery, Colorado State University, Fort Collins, CO 80523, USA

[5]Lead contact

SUMMARY

Strategies for slowing magnetic relaxation via local environmental design are vital for developing next-generation spin-based technologies (e.g., quantum information processing). Herein, we demonstrate a technique to do so via chemical design of a local magnetic environment. We show that embedding the open-shell complex $(Ph_4P)_2[Co(SPh)_4]$ in solid-state matrices of the isostructural, open-shell species $(Ph_4P)_2[M(SPh)_4]$ (M = Ni^{2+}, $S = 1$; M = Fe^{2+}, $S = 2$; M = Mn^{2+},$S = {}^5/_2$) will slow magnetic relaxation for the embedded $[Co(SPh)_4]^{2-}$ ion by three orders of magnitude. Magnetometry, electron paramagnetic resonance (EPR), and computational analyses reveal that integer spin and large, positive zero-field splitting (D) values for the diluent produce a quiet, local magnetic field that slows relaxation rates for the embedded Co molecules. These results will enable the investigation of magnetic systems for which strictly diamagnetic congeners are either synthetically inaccessible or are not isostructural.

Graphical Abstract

*Correspondence: joe.zadrozny@colostate.edu.

AUTHOR CONTRIBUTIONS

J.M.Z. and I.P.M. conceived of the experiments. I.P.M., A.O., and J.A.D. executed the experiments. H.C. and C.P.A. conceived of and executed the simulations. All authors were involved in data analysis and writing the manuscript.

DECLARATION OF INTERESTS

The authors declare no competing interests.

SUPPLEMENTAL INFORMATION

supplemental information can be found online at https://doi.org/10.1016/j.xcrp.2022.100802.

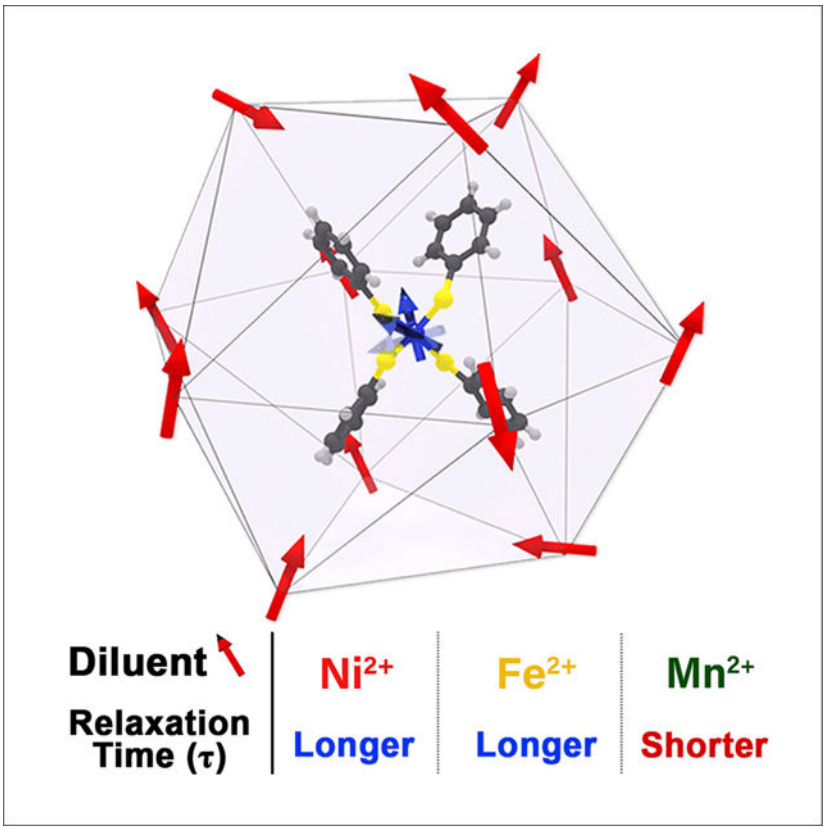

Moseley et al. show, via paramagnetic dilution, that the single-ion magnet $[Co(SPh)_4]^{2-}$ exhibits slowed spin relaxation in paramagnetic matrices if the environment is specially designed. This result may have implications for future magnetic analysis experiments.

INTRODUCTION

Single-molecule magnets are potential next-generation components in information storage/processing,[1–3] spintronics,[4] and magnetic resonance imaging.[5] These complexes display an activation energy barrier (U) to reorientation of the magnetic moment that can induce extremely long magnetic relaxation times (τ > s) at low temperature.[6–12] Environmental spins (which constitute the "spin bath") frequently induce rapid relaxation through dipolar interactions, and nearly all envisioned applications of single-ion magnets (the mononuclear family of single-molecule magnets) involve the existence of a spin bath in some form (e.g., high-density arrays of open-shell molecules on surfaces or ^{1}H nuclear-spin-rich aqueous environments).[13] Hence, developing new ways to study, understand, and chemically control the impact of the spin bath on relaxation is vital to eventual application.

At low temperatures, the spin bath of a metal ion hastens relaxation by enhancing quantum tunneling of the magnetization.[14] In this process, a single-ion magnet's spin will flip and undercut the barrier.[15] Tunneling in these systems is typically driven by dipolar interactions with adjacent molecules and can be disrupted by diamagnetic dilution.[1,16] Diamagnetic dilution is achieved by taking a magnetic molecule and either (1) dissolving it into an

organic solvent or matrix (as was done for $Mn_{12}O_{12}$),[17,18] or (2) cocrystallization with a structurally analogous, closed-shell species. For example, mononuclear M^{2+} complexes can be diluted with Zn^{2+}[19] or low-spin Ni^{2+} analogues[20]; M^{3+} species can be diluted with low-spin Co^{3+},[21] Y^{3+},[22,23] or Ga^{3+}[24]; and M^{4+} species can be diluted with Ti^{4+}.[25] In these dilute systems, wherein the size advantage of high-density molecular information storage is lost, magnetic relaxation is often slowed by several orders of magnitude. It is vital to deviate away from these magnetically quiet confines to discover how to slow relaxation rates when the environment is noisy. Thus, it is essential to develop new, chemical means of modifying the local magnetic environment to study mechanisms of magnetic relaxation.

Herein, we illustrate a way of chemically manipulating relaxation via cocrystallization within a synthetically tunable paramagnetic matrix. Importantly, we use this method to show that select $S = 1$ and $S = 2$ ions can produce a spin bath that suppresses tunneling similar to a bath of closed-shell Zn^{2+}, yet still possessing unpaired electrons. This work focuses on the single-ion magnet $[Co(SPh)_4]^{2-}$ (Figure 1), which demonstrates facile quantum tunneling at low temperature in the pure phase.[19] We measured the magnetization dynamics of dilutions of $(Ph_4P)_2[Co(SPh)_4]$ (Co, $S = 3/2$) in the paramagnetic diluents $(Ph_4P)_2[Ni(SPh)_4]$ (Ni, $S = 1$), $(Ph_4P)_2[Fe(SPh)_4]$ (Fe, $S = 2$), $(Ph_4P)_2[Mn(SPh)_4]$ (Mn, $S = 5/2$), and the diamagnetic diluent $(Ph_4P)_2[Zn(SPh)_4]$ (Zn, $S = 0$). These data reveal an exciting disruption of tunneling for baths of $S = 1$ Ni and $S = 2$ Fe, like the effects observed for the traditional diamagnetic diluent $S = 0$ Zn. Through EPR, susceptibility, and theoretical modeling data, we correlate the viability of the $S = 1$ Ni and $S = 2$ Fe diluents with the positive zero-field splitting (D) of these species (see Note S2). This feature, we propose, makes them effective-spin zero ($S_{eff} = 0$) at low temperature despite possessing multiple unpaired electrons (unlike Zn^{2+}) and effectively quiets the local dipolar fields that hasten relaxation.[26,27] Although most dilutions of single-molecule magnets exploit strictly diamagnetic environments, this study is, to the best of our knowledge, the first to explicitly target magnetically concentrated diluting conditions.

RESULTS AND DISCUSSION

Synthesis

The $(Ph_4P)_2[M(SPh)_4]$ species (M = Mn, Fe, Co, Ni, and Zn), denoted Mn, Fe, Co, Ni, and Zn, respectively, are isostructural mononuclear complexes.[28,29] A tetragonal elongation in the tetrahedral MS_4 unit of these complexes makes the local symmetry D_{2d} and engenders an extreme magnetic anisotropy and slow magnetic relaxation for Co.[30] A slight change is observed in the average M–S distances as a function of M (2.328(4) for Co,[29] 2.288(4) for Ni,[28] 2.356(6) for Fe,[29] 2.442(3) for Mn, and 2.352(3) Å for Zn),[28] but all crystallize in the $Pbc2_1$ space group. Furthermore, the same tetragonal distortion toward D_{2d} symmetry is seen in all $[M(SPh)_4]^{2-}$ units, with two S–M–S angles exhibiting a “pinch” as a function of the elongation. These pinched S–M–S angles are 96.7(2)° (Zn), 92.0(2)° (Ni), 95.6(2)° (Co), 97.58(10)° (Fe), and 98.4(1)° (Mn). We note that these specific bond angles are bisected by the magnetic easy-axis of the $[Co(SPh)_4]^{2-}$ unit in Co. Finally, each metal ion has 12 nearest neighbors, with closest M···M distances of around 10.456(7) Å (Figure 1).[25,28]

Multiple sets of solid solutions of Co in Ni, Fe, Mn, and Zn were made to test the impact of paramagnetic spin baths on magnetic relaxation of Co. First, we prepared variable concentrations of Co in Ni (73%, 58%, 25%, 9%, and 3% Co relative to Ni). Second, we prepared dilutions of Co in Fe (83%, 57%, 24%, 16%, and 6% Co to Fe). Third, dilutions of Co in Mn (81% and 43% Co to Mn) and, finally, dilutions of Co in Zn (30% and 3% Co to Zn). Powder X-ray diffraction (PXRD) patterns demonstrate that these dilutions assume the same crystalline phases of their pure components, and preliminary energy-dispersive X-ray spectroscopy (EDS) data suggest homogeneous distribution over micrometer-length scales (see Note S1, supplemental experimental procedures and Figures S1 and S2).[31]

Direct current susceptibility

Magnetic analyses via direct-current (dc) magnetic susceptibility ($\chi_M T$) measurements indicate that Co, Ni, Fe, and Mn are isolated spin systems with varying magnetic anisotropies. Room temperature (300 K) $\chi_M T$ values of 2.45, 1.34, 2.90, and 4.56 cm^3K/mol for Co, Ni, Fe, and Mn (Figure S3) indicate $S = {}^3/_2$, 1, 2, and ${}^5/_2$ metal ions, respectively, matching previous results.[32] With decreasing temperature, $\chi_M T$ decreases, most likely a result of the zero-field splitting. This decrease is most dramatic for Ni, less so for Co and Fe, and almost negligible for Mn. The $\chi_M T$ data were fit with a spin Hamiltonian accounting for zero-field splitting (using the program PHI[33]; see supplemental information for fitting details). The final extracted D values are $D \approx -61$ for Co, $D = +68\ cm^{-1}$ for Ni, $D = +5.85\ cm^{-1}$ for Fe, and $D = -0.12\ cm^{-1}$ for Mn; all values are in keeping with previous reports for other similar, four-coordinate MS_4 complexes.[34–37]

High-field, high-frequency EPR

Electron paramagnetic resonance (EPR) measurements were pursued to better quantitate the zero-field splitting for Mn, Fe, and Ni (Figures 2 and S4–S7), as dc susceptibility can sometimes incorrectly assign the signs/magnitudes of these parameters.[38] High-field and high-frequency EPR (HF-EPR) analyses of Co were previously reported and generally agree with the large, negative D obtained from dc susceptibility fits.[30] For Ni and Fe, which also appeared by $\chi_M T$ to have large D values, we used high-field (up to 17 T) and high-frequency analyses (up to 650 GHz). For Fe, a highly frequency- and temperature-dependent EPR spectrum was observed, with multiple sharp peaks detected at all frequencies (see Figures 2 and S4–S6). In contrast, no EPR signal was observed for Ni from 0 to 17 T and frequencies up to 650 GHz.

The EPR spectra generally agree with the susceptibility analyses and were simulated with Easyspin[39] and the program *SPIN* (see Table S1 and supplemental information for full details). First, for $S = 1$ Ni with a D of ca. $+67\ cm^{-1}$, we observed, as expected, no EPR signal under the experimental fields and frequencies. Second, for Fe ($S = 2$), relatively sharp, well-resolved peaks were observed, and the frequency/field dependence of these peaks can be convincingly modeled with $D = +5.848(1)\ cm^{-1}$, and $E = +1.428(1)\ cm^{-1}$, in general agreement with other lower-frequency EPR analyses (Figure 2).[40–42] Finally, for Mn, simulations of the 381-GHz spectra produce average D and E values of $-0.12\ cm^{-1}$, and $-0.04\ cm^{-1}$, respectively, close to the small values from $\chi_M T$ simulations (Figure S7) and the general expectations for an Mn^{2+} ion.[43–45]

Modeling the HF-EPR spectra of Fe and Mn was attempted for both positive and negative values of the anisotropy parameters (D and E). The models for Fe obtained when $D > 0$ resulted in significant improvements over the model with $D < 0$ (Figure S6). In the case of Mn, which possesses a much smaller zero-field splitting and higher rhombicity ($E/D \approx 0.3$), the simulations of the HF-EPR spectra were of generally equal quality with negative or positive D.

Together, the susceptibility and EPR data highlight an important varying aspect of the different bath spins, beyond just S: the ground-state M_S values (Figure 2). The large positive D for Ni suggests that the $M_S = 0$ level of Ni bath spins is the lowest energy and separated from the $M_S = \pm 1$ levels by a ~67 cm^{-1} gap. The data for Fe likewise indicate that the Fe^{2+} ions possess a ground $M_S = 0$ level. However, the $M_S = 0$ level is only separated by ~3 cm^{-1} from the $M_S = \pm 1$ levels and ~24 cm^{-1} from the $M_S = \pm 2$ levels for Fe relative to the 67 cm^{-1} gap for Ni. Note that the $M_S = \pm 1$ levels are split for Fe by a transverse anisotropy $|E| = 1.43$ cm^{-1}, and this anisotropy also mixes these levels. For Mn, the separation in all M_S levels is even smaller, with the $M_S = \pm 5/2$ levels separated from the $M_S = \pm ½$ levels by 0.88 cm^{-1} (Figure 2). As is shown below, these specific arrangements of M_S levels are critical to the respective roles of Mn, Ni, and Fe as diluents for Co.

Alternating-current susceptibility

Out-of-phase, alternating-current (ac) magnetic susceptibility (χ_M'') measurements of pure Co, Ni, Fe, and Mn reveal slow magnetic relaxation at zero applied dc field for only Co at ac frequencies from 0.1 to 1,500 Hz. For Co, we observe a nonzero, frequency-dependent χ_M'' with a peak at 27.7 Hz at 2.0 K (Figure S8). From 2 to 2.6 K, the frequency of this peak is temperature independent, indicative of quantum tunneling. In contrast, above 3.0 K, the peak position is highly temperature dependent. This behavior is typical of magnetic relaxation that transitions to thermally activated processes.[19,46] In contrast Ni, Fe, and Mn display a featureless χ_M'' at zero applied dc field (Figure S9). The only indication of slow magnetic relaxation in these latter compounds is in Mn, which shows a high-frequency rise in χ_M'' (200–1,000 Hz) under 500–1,500 G applied fields, but a peak maximum is never fully resolved (Figure S10). These data establish the zero-field ac susceptibility measurement as an effective probe of the dynamics of Co alone in the three probed spin baths (composed of Ni, Fe, and Mn), owing to the absence of a zero-field χ_M'' signal in these diluents.

Zero-field ac magnetic susceptibility studies of Co diluted to different extents in Ni (Figures 3, and S11–S13) reveal a slowing of magnetic relaxation at 2 K upon dilution in the $S = 1$ bath. For pure Co, there is a region of temperature independence in χ_M'' below 2.5 K when no external field is applied, an indication of magnetic dipole-mediated tunneling relaxation processes. In contrast, for the dilutions, magnetic relaxation is increasingly temperature dependent below 2.5 K with increasing dilution level, indicating that the tunneling process is disfavored in the diluted samples. Furthermore, the χ_M'' peaks for Co broaden at low temperature when diluted, an additional indicator that the dilution process is effectively modulating the tunneling-based magnetic relaxation in the $T < 3$ K temperature regime (Tables S4–S5).

Quantitation of the relaxation times (τ) from a Cole-Cole analysis[47] of the ac data enabled the construction of Arrhenius plots (Figure 3) for the relaxation dynamics of Co in Ni. For pure Co, τ is temperature independent from 2.0 to 2.6 K at a value of ca. 36 ms (Figure S8). The values of τ become longer over this temperature window and generally more temperature dependent with increasing dilution level in Ni. The parameter α, which is also obtained from the Cole-Cole fitting (and characterizes the broadness of the χ_M'' peak), increases from 0.276 at 2.0 K for pure Co to 0.579 at 2.0 K for the 1:34 Co:Ni dilution. A larger value of α in the Cole-Cole analysis suggests a larger distribution of relaxation times for the Co unit upon dilution in Ni, which is likely because of some inhomogeneity in the disruption of the tunneling process.

The variable-temperature τ data for pure Co can be easily modeled with two common magnetic relaxation processes, Raman and quantum tunneling,[15,48] via the following equation: $1/\tau = A T^n + 1/\tau_{QTM}$ (see Table S2–S3; Figure S14 for full details). Here, $1/\tau$ is the relaxation rate, A is the Raman coefficient related to physical properties of the crystal, n is the Raman exponent, T is temperature, and τ_{QTM} is the timescale of the quantum tunneling of the magnetization. As a function of dilution, the best fits change, most notably for the tunneling process, which slows considerably, with τ_{QTM} = 6.6(4) ms for pure Co lengthening to τ_{QTM} = 41(3) ms for 1:2 Co:Ni (Table S2; Figures 3 and S15). These data indicate a slowing of magnetic relaxation via reduction of tunneling with increasing Ni concentration, just like dilution with Zn.[19] At higher dilutions, tunneling is no longer required to simulate the data, which can be modeled solely with a Raman process. The parameters for the Raman process change upon dilution, with A ranging from 0.03(1) to 0.8(2) $K^{-n}s^{-1}$ and n = 5.6(1) to 7.96(9) for Co:Ni dilutions. The Raman process is predicted to be dependent on dipolar interaction.[48] These data may thus provide the first quantitative evidence of the spin-bath impact on Raman relaxation; however, caution should be exercised in analyzing this change too deeply as the present analysis only spans a 5 K window of relaxation dynamics.

Additional variable-concentration ac susceptibility analyses of the dilutions of Co in $S = 2$ Fe, $S = 5/2$ Mn, and S = 0 Zn were performed to test the effect of the different paramagnetic baths (Figures 4 and S11–S19). Zero-field, 2 K analyses of dilutions with Fe demonstrate a similar effect as Ni and Zn, in that increasing concentration of the diluent slows the relaxation rate of Co and the χ_M'' peaks broaden considerably. Importantly, however, Fe appears slightly less effective as a diluent than Ni, as the relaxation rates for Co appear faster in the Fe diluent at all studied concentrations. Just like with Fe and Ni, the peak in χ_M'' for Co when diluted in Mn becomes broadened in frequency space, indicating a distribution in relaxation times. However, in contrast to Fe and Ni, the χ_M'' peak maximum for Co in Mn rapidly moves to higher frequencies with increasing Mn concentration, indicating relaxation rates that rapidly hasten beyond the detectable range of our magnetometer.

The presented relaxation time data suggest that the functional feature of the Fe and Ni spin baths is related to the magnetic anisotropy of the spin-bath ions. For an integerspin ion with a positive D (e.g., Ni and Fe), the ground M_S levels are $M_S = 0$ and bear no spin angular momentum. Note that this scenario is distinct from being completely diamagnetic, as both Fe and Ni still possess unpaired electrons (i.e., they are not undergoing a low-temperature

spin crossover),[49] and there is no zero-field splitting for an $S = 0$ spin state. At 2 K, the 67 cm^{-1} energy gap between the $M_S = 0$ and ±1 levels in Ni is significant, and the $M_S = 0$ level is populated by nearly 100% of the spins in the Ni bath (following a simple Boltzmann distribution). Hence, to the magnetization dynamics of Co ions embedded in the Ni bath, this" effective $S = 0$" state for Ni appears to wield the same impact as the $S = 0$ Zn bath, despite Ni being an open-shell complex and Zn closed shell. Fe is also an integer spin with positive D, and hence it shows a similar effect on the quantum tunneling process for Co, owing to a high population of the $M_S = 0$ level (73%). However, the data in Figure 4 demonstrate that Fe does not disrupt the tunneling process as effectively as Ni, as the relaxation rates for Co diluted in Fe are faster than when diluted in Ni at all measured concentrations. To explain this discrepancy, we note that the D of Fe is smaller than that of Ni by a factor of 11.7. This smaller D (and the appreciable E) for Fe means that one of the $M_S = \pm 1$ levels is populated by 26% at 2 K. Hence, Fe is less effective as a diluent because there is sufficient population of the magnetic $M_S \neq 0$ levels at 2 K, and the spin bath can hence induce quantum tunneling for Co. This explanation mirrors previous work by Cornia and coworkers on chain compounds, which showed that integerspin ions with strong easy-plane anisotropy incorporated into chains of open-shell species will block intrachain exchange interactions.[50]

In contrast to Fe and Ni, dilutions of with Mn hastened the relaxation time for embedded Co. For half-integer, high-spin ions (e.g., Mn), no matter the sign of D, the ground M_S levels are either $M_S = \pm ½$ or $M_S = \pm 5/2$ for the ion; both configurations are magnetic, and the small D suggests that, even in the low-T regime, all M_S levels will be populated. As a result, Mn provides a strongly magnetic local environment to drive tunneling beyond what is typical for pure Co.

Dipolar field calculations

Intermolecular dipole-dipole forces strongly influence the rate of quantum tunneling for mononuclear single-molecule magnets, and it is known that both axial ($H^{dip}_{\parallel}$) and transverse ($H^{dip}_{\perp}$) dipolar fields increase the rate of tunneling.[51,52] We hypothesized that the positive D of Ni and Fe would subdue the magnitudes of dipolar fields, which would suppress tunneling to enable slow relaxation rates. To test this hypothesis and characterize the local dipolar field created by the paramagnetic diluents, we estimated the local magnetic dipolar field of a Co embedded in matrices of Mn, Co, Ni, and Zn, using g, D, and S values from EPR and $\chi_M T$ analyses for the diluting molecules (Figure 5). We note the general results of Ni can likely be extended to the analogous, positive-D, integerspin Fe. We assumed that the dipolar field $\boldsymbol{h}$ can be approximated by a zero-mean Gauss-Markov stochastic process fully characterized by its autocorrelation function with variance $c_h^n \equiv \langle h_n h_n \rangle$, with $n = x, y, z$, and decay rate Γ_h, in the spirit of the Kubo-Toyabe theory of zero-field spin relaxation.[53] c_h^n serves as a measure of the fluctuating $\boldsymbol{h}$ and is related to the Co spin relaxation time τ as detailed in Note S3. c_h^n can then be calculated from the static spin-spin correlation function of the bath spins, which are assumed to be independent as a first approximation. We selected x, y, and z to be coincident with the zero-field splitting axes of the embedded Co species,

taken from the crystal structure. Detailed computational methods and results can be found in Note S3 and Figures S22 and S23.

The dipolar fields imparted on an embedded Co are anisotropic, shown by the different magnitudes of c_h^x, c_h^y, and c_h^z. For example, at 2.2 K, pure Ni produces c_h^x, c_h^y, and c_h^z magnitudes of 0.32, 0.32, and 0.21 mT^2 respectively. This anisotropy stems from the relative orientations of the surrounding spins since the molecular axes of each of the four $[M(SPh)_4]^{2-}$ species in the unit cell are not aligned in the crystal structure (Figure S24). We also determined that the field strength is not dependent on which molecular site we choose as the origin, provided that the x, y, and z axes are defined according to the molecular axes of that site.

More importantly, the calculated c_h^n have different magnitudes for different bath spins, especially at low temperatures. In contrast to the values for pure Ni mentioned above, we found that at 2.2 K the c_h^x, c_h^y, and c_h^z in pure Co ($S = 3/2$) are much larger, 32.9, 34.4, and 21.9 mT^2, respectively, and those in Mn ($S = 5/2$) are even larger: 50.2, 51.9, and 45.8 mT^2, respectively (Figures 5C and S22). The fluctuating dipolar fields for the half-integerspin baths are therefore one order of magnitude larger than that for the integerspin bath (Ni) at low temperatures, in agreement with our qualitative picture above. That the c_h^n for Mn is larger than that for Co is mainly due to the larger spin of the former. A complete description of the observed trends can be found in Note S3.

Since the very small c_h^n for pure Ni is a result of the dominant occupancy of the $M_S = 0$ singlet at low temperatures, we expect that c_h^n will undergo a nontrivial transition upon increasing temperature. Indeed, Figure 5A shows that c_h^n changes significantly around $T = 10$ K, where $\chi_M T$ exhibits the sharpest increase (Figure S3), again caused by the zero-field splitting of Ni. Specifically, c_h^x dramatically drops from 41 mT^2 at 25 K to 0.32 mT^2 at 2.5 K, a 99% decrease, with c_h^y and c_h^z behaving similarly. In contrast, the c_h^n for Co and Mn have much milder temperature dependence in the same temperature range (Figure S22). For Co, two of the components, c_h^x and c_h^y, increase with decreasing temperature from 50 to 2.2 K, but not dramatically, and level off at 32.9 and 34.4 mT^2 at 2.2 K, respectively. In contrast, c_h^z decreases for Co with decreasing temperature, eventually reaching 21.9 mT^2 at 2.2 K. Mn is similar to Co, except there is only a pronounced temperature dependence below approximately 0.5 K, consistent with the extremely small zero-field splitting.

With increasing dilution, both the local field magnitude and its temperature dependence gradually change from that of pure Co to that of the diluent, as shown in Figure 5B for the case of Co in Ni. At a fixed temperature, we found that c_h^n depends linearly on the dilution for all baths (Figures 5C and S23), a consequence of our independent bath spin assumption. The nice agreement between the linear dependences of c_h^n and the experimental $1/\tau$ data on dilution confirms the applicability of this assumption.

The observed orientation, temperature, and diluent dependence of the local dipolar fields are all in agreement with our interpretation of the effect of the different $[M(SPh)_4]^{2-}$ environments. Importantly, the possibility of structural changes to $[Co(SPh)_4]^{2-}$ via chemical pressure is ruled out via comparison of structural changes and predicted effects (see supplemental information). Thus, we see the operative mechanism of the Ni and Fe diluents. The $M_S = 0$ level is almost entirely populated at low temperature, causing all dipolar fields to fall to 0. This reduction of the dipolar field then suppresses the tunneling relaxation, as observed for diamagnetic Zn dilution. Furthermore, we see why Co and Mn both enable tunneling of embedded Co species: the half-integer spins of these bath complexes (in contrast to the integerspin, positive-D Ni) ensure that a substantial, nonzero dipolar field (Mn larger than Co) exists at low temperature. Consequently, we see tunneling proceed in pure Co and the relaxation rate increase when dilute in Mn. Note that although c_h^n is an indicator of how noisy the spin bath is magnetically, it does not have a simple proportionality relationship with the Co spin relaxation rate, which depends on complex kinetic processes involving many spins coupled by dipolar interaction. Nonetheless, the temperature dependence of c_h^n for Ni qualitatively agrees with the trend of the experimental relaxation rate at low temperatures (Figure 3).

The foregoing dilutions harness zero-field splitting to suppress dipolar field fluctuations and slow relaxation. In this context, the demonstrated dilutions expand a lineup of possibilities for exploiting magnetic interactions to reduce environmental noise. For example, antiferromagnetically coupled dicopper complexes, despite possessing 2 $S = ½$ Cu^{2+} ions, will produce magnetically quiet environments at low temperature and enable the observation of relatively sharp EPR spectra.[54–56] We also anticipate that other interactions may work to produce new families of diluents. Dilutions using Eu^{3+} may be possible for rare-earth ions, where spin orbit coupling between the $L = 3$ and $S = 3$ of the Eu^{3+} ion cancel to yield a magnetically quiet $J = 0$ state.[57]

This demonstration is the first slowing of the magnetization dynamics of a single-molecule magnet by deliberate chemical dilution with an open-shell diluent. Our results reveal that $S = 1$ and $S = 2$ complexes can be used to reduce quantum tunneling of the magnetization, like $S = 0$ analogues, if D is positive and of sufficient magnitude.

One implication of these results is the ability to magnetically dilute with open-shell complexes, which may be useful when closed-shell analogues are chemically unstable or non-isostructural, as, for example, radical-bridged bimetallic species[58] or systems where the diluent and ion of interest have substantially different ionic radii. There is an enormous diversity of metal ions, spin states, and geometries that produce positive zero-field splitting,[59] and thus we hope this result will open the door substantially for what is possible for achieving effective dilutions.

Second, although the diluents still create a magnetically silent environment, the unpaired electrons of these bath spins are still potentially addressable via spin resonance methods. Hence, materials based of the presented design strategies may enable tests of the needed

multi-spin manipulations (and associated relaxation processes) in high-density arrays, a necessary capability for spin-based quantum computation.[2,3]

Finally, we note that this work describes the impact of magnetic baths on a single-molecule magnet with easy-axis magnetic anisotropy, for which quantum tunneling is the dominant relaxation mechanism. There are many other relaxation mechanisms that are predicted to be affected by dipolar fields, but these predictions have yet to be quantitatively tested.[60–62] Future work will test these theories with the paramagnetic dilution approach, and those results will be presented in due course.

EXPERIMENTAL PROCEDURES

Resource availability

Lead contact—Further information and requests for resources should be directed to and will be fulfilled by the lead contact, Joseph Zadrozny (joe.zadrozny@colostate.edu).

Materials availability: All materials generated in this study are available from the lead contact upon request.

Data and code availability: Datasets generated during this study are available upon request.

General methods

Detailed syntheses, magnetic analyses, and additional spectroscopic data and interpretation can be found in the supplemental experimental procedures.

Supplementary Material

Refer to Web version on PubMed Central for supplementary material.

ACKNOWLEDGMENTS

We acknowledge Profs. N. Prokof'ev, and A. Kent for fruitful discussions. This research was performed with the support of Colorado State University and the National Science Foundation (CHE-1836537). Magnetization experiments were performed at the CSU Central Instrument Facility, which is supported by an NIH-SIG award (1S10OD021814-01) and the CSU-CORES Program. A portion of this work was performed at the National High Magnetic Field Laboratory, which is supported by the National Science Foundation Cooperative Agreement no. DMR-1644779 and the State of Florida. C.A. and H.C. were partially supported by NSF CAREER grant DMR-1945023. This material is based on work supported by the National Science Foundation Graduate Research Fellowship under grant no. 006784-00002.

REFERENCES

1. Gatteschi D, Sessoli R, and Villain J (2006). Molecular Nanomagnets (Oxford University Press).
2. Lehmann J, Gaita-Ariño A, Coronado E, and Loss D (2009). Quantum computing with molecular spin systems. J. Mater. Chem. 19, 1672–1677.
3. Aromí G, Aguilà D, Gamez P, Luis F, and Roubeau O (2012). Design of magnetic coordination complexes for quantum computing. Chem. Soc. Rev. 41, 537–546. [PubMed: 21818467]
4. Thiele S, Balestro F, Ballou R, Klyatskaya S, Ruben M, and Wernsdorfer W (2014). Electrically driven nuclear spin resonance in single-molecule magnets. Science 344, 1135–1138. [PubMed: 24904159]

5. Wahsner J, Gale EM, Rodríguez-Rodríguez A, and Caravan P (2019). Chemistry of MRI contrast agents: current challenges and new frontiers. Chem. Rev. 119, 957–1057. [PubMed: 30350585]
6. Rechkemmer Y, Breitgoff FD, Van Der Meer M, Atanasov M, Hakl M, Orlita M, Neugebauer P, Neese F, Sarkar B, and Van Slageren J (2016). A four-coordinate cobalt(II) single-ion magnet with coercivity and a very high energy barrier. Nat. Commun. 7, 1–8.
7. Latendresse TP, Bhuvanesh NS, and Nippe M (2017). Slow magnetic relaxation in a lanthanide-[1]metallocenophane complex. J. Am. Chem. Soc. 139, 8058–8061. [PubMed: 28590123]
8. Cardona-Serra S, Clemente-Juan JM, Coronado E, Gaita-Ariño A, Camón A, Evangelisti M, Luis F, Martínez-Pérez MJ, and Sesé J (2012). Lanthanoid single-ion magnets based on polyoxometalates with a 5-fold symmetry: the series $[LnP_5W_{30}O_{110}]^{12-}$ (Ln^{3+} = Tb, Dy, Ho, Er, Tm, and Yb). J. Am. Chem. Soc. 134, 14982–14990. [PubMed: 22894703]
9. Chen YC, Liu JL, Ungur L, Liu J, Li QW, Wang LF, Ni ZP, Chibotaru LF, Chen XM, and Tong ML (2016). Symmetry-supported magnetic blocking at 20 K in pentagonal bipyramidal Dy(III) single-ion magnets. J. Am. Chem. Soc. 138, 2829–2837. [PubMed: 26883386]
10. Ishikawa N, Sugita M, Ishikawa T, Koshihara SY, and Kaizu Y (2003). Lanthanide double-decker complexes functioning as magnets at the single-molecular level. J. Am. Chem. Soc. 125, 8694–8695. [PubMed: 12862442]
11. Guo F-S, Day BM, Chen Y-C, Tong M-L, Mansikkamäki A, and Layfield RA (2018). Magnetic hysteresis up to 80 kelvin in a dysprosium metallocene single-molecule magnet. Science 362, 1400–1403. [PubMed: 30337456]
12. Goodwin CAP, Ortu F, Reta D, Chilton NF, and Mills DP (2017). Molecular magnetic hysteresis at 60 kelvin in dysprosocenium. Nature 548, 439–442. [PubMed: 28836589]
13. Berliner LJ, Eaton GR, and Eaton SS (2002). In Distance Measurements in Biological Systems by Berliner EPRLJ, Eaton GR and Eaton SS, eds. (Springer US).
14. Garanin DA (2012). Dipolar-controlled spin tunneling and relaxation in molecular magnets. Eur. Phys. J. B 85, 1–10.
15. Gatteschi D, and Sessoli R (2003). Quantum tunneling of magnetization and related phenomena in molecular materials. Angew. Chem. Int. Ed. Engl. 42, 268–297. [PubMed: 12548682]
16. Vergnani L, Barra AL, Neugebauer P, Rodriguez-Douton MJ, Sessoli R, Sorace L, Wernsdorfer W, and Cornia A (2012). Magnetic bistability of isolated giant-spin centers in a diamagnetic crystalline matrix. Chem. A Eur. J. 18, 3390–3398.
17. Sessoli R, Gatteschi D, Caneschi A, and Novak MA (1993). Magnetic bistability in a metal-ion cluster. Nature 365, 141–143.
18. Sessoli R, Tsai H-L, Schake AR, Wang S, Vincent JB, Folting K, Gatteschi D, Christou G, and Hendrickson DN (1993). High-spin molecules. J. Am. Chem. Soc. 115, 1804–1816.
19. Zadrozny JM, and Long JR (2011). Slow magnetic relaxation at zero field in the tetrahedral complex $[Co(SPh)_4]^{2-}$. J. Am. Chem. Soc. 133, 20732–20734. [PubMed: 22142241]
20. Attanasio D, Collamati I, and Daul C (2005). EPR properties of a cobalt(II) complex containing a low-symmetry porphyrin-like ligand. Inorg. Chem. 24, 2746–2750.
21. Bhowmick I, Roehl AJ, Neilson JR, Rappé AK, and Shores MP (2018). Slow magnetic relaxation in octahedral low-spin Ni(III) complexes. Chem. Sci. 9, 6564–6571. [PubMed: 30310588]
22. Habib F, Lin PH, Long J, Korobkov I, Wernsdorfer W, and Murugesu M (2011). The use of magnetic dilution to elucidate the slow magnetic relaxation effects of a Dy2 single-molecule magnet. J. Am. Chem. Soc. 133, 8830–8833. [PubMed: 21563820]
23. Luis F, Martínez-Pérez MJ, Montero O, Coronado E, Cardona-Serra S, Martí-Gastaldo C, Clemente-Juan JM, Sesé J, Drung D, and Schurig T (2010). Spin-lattice relaxation via quantum tunneling in an Er^{3+}-polyoxometalate molecular magnet. Phys. Rev. B Condens. Matter 82, 3–6.
24. Zadrozny JM, and Freedman DE (2015). Qubit control limited by spin-lattice relaxation in a nuclear spin-free iron(III) complex. Inorg. Chem. 54, 12027–12031. [PubMed: 26650962]
25. Stinghen D, Atzori M, Fernandes CM, Ribeiro RR, De Sá EL, Back DF, Giese SOK, Hughes DL, Nunes GG, Morra E, et al. (2018). A rare example of four-coordinate nonoxido vanadium(IV) alkoxide in the solid state: structure, spectroscopy, and magnetization dynamics. Inorg. Chem. 57, 11393–11403. [PubMed: 30160486]

26. Atanasov M, Aravena D, Suturina E, Bill E, Maganas D, and Neese F (2015). First principles approach to the electronic structure, magnetic anisotropy and spin relaxation in mononuclear 3d-transition metal single molecule magnets. Coord. Chem. Rev. 289–290, 177–214.
27. Campochiaro C, Pavel EG, and Solomon EI (1995). Saturation magnetization magnetic circular dichroism spectroscopy of systems with positive zero-field splittings: application to $FeSiF_6{\cdot}6H_2O$. Inorg. Chem. 34, 4669–4675.
28. Swenson D, Baenziger NC, and Coucouvanis D (1978). Tetrahedral Mercaptide complexes. Crystal and molecular structures of $[(C_6H_5)_4P]_2M(SC_6H_5)_4$ complexes (M= Cd(II), Zn(II), Ni(II), Co(II), and Mn(II)). J. Am. Chem. Soc. 100, 1932–1934.
29. Coucouvanis D, Swenson D, Baenziger NC, Holah DG, Kostikas A, Simopoulos A, and Petrouleas V (1976). The crystal and molecular structures of $[(C_6H_5)_4P]_2Fe(S_2C_4O_2)_2$ and $[(C_6H_5)_4P]_2Fe(SC_6H5)_4$, a structural analogue of reduced rubredoxin. J. Am. Chem. Soc. 98, 5721–5723. [PubMed: 956577]
30. Suturina EA, Nehrkorn J, Zadrozny JM, Liu J, Atanasov M, Weyhermüller T, Maganas D, Hill S, Schnegg A, Eckhard B, et al. (2017). Magneto-structural correlations in pseudotetrahedral forms of the $[Co(SPh)_4]^{2-}$ complex probed by magnetometry, MCD spectroscopy, advanced EPR techniques, and ab initio electronic structure calculations. Inorg. Chem. 56, 3102–3118. [PubMed: 28225611]
31. Shindo D, and Oikawa T (2002). Energy dispersive X-ray spectroscopy. In Analytical Electron Microscopy for Materials Science (Springer Japan), pp. 81–102.
32. Holah DG, and Coucouvanis D (1975). Synthesis and characterization of a new series of first row element tetrahedral mercaptide complexes. J. Am. Chem. Soc. 97, 6917–6919.
33. Chilton NF, Anderson RP, Turner LD, Soncini A, and Murray KS (2013). PHI: a powerful new program for the analysis of anisotropic monomeric and exchange-coupled polynuclear d- and f-block complexes. J. Comput. Chem. 34, 1164–1175. [PubMed: 23386394]
34. Sottini S, Poneti G, Ciattini S, Levesanos N, Ferentinos E, Krzystek J, Sorace L, and Kyritsis P (2016). Magnetic anisotropy of tetrahedral CoII single-ion magnets: solid-state effects. Inorg. Chem. 55, 9537–9548. [PubMed: 27636564]
35. Hawrelak EJ, Bernskoetter WH, Lobkovsky E, Yee GT, Eckhard B, and Chirik PJ (2005). Square planar vs tetrahedral geometry in four coordinate iron(II) complexes. Inorg. Chem. 44, 3103–3111. [PubMed: 15847415]
36. Cirera J, Ruiz E, Alvarez S, Neese F, and Kortus J (2009). How to build molecules with large magnetic anisotropy. Chem. A Eur. J. 15, 4078–4087.
37. Kowal AT, LeGall J, Johnson MK, Zambrano IC, Moura I, and Moura JJG (1988). Electronic and magnetic properties of nickel-substituted rubredoxin: a variable-temperature magnetic circular dichroism study. Inorg. Chem. 27, 1162–1166.
38. Kahn O (1993). Molecular Magnetism (VCH).
39. Stoll S, and Schweiger A (2006). EasySpin, a comprehensive software package for spectral simulation and analysis in EPR. J. Magn. Reson. 178, 42–55. [PubMed: 16188474]
40. Boča R (2004). Zero-field splitting in metal complexes. Coord. Chem. Rev. 248, 757–815.
41. Bendix J, Brorson M, and Schäffer CE (1993). Accurate empirical spin-orbit coupling parameters znd for gaseous ndq transition metal ions. The parametrical multiplet term model. Inorg. Chem. 32, 2838–2849.
42. Knapp MJ, Krzystek J, Brunel LC, and Hendrickson DN (2000). High-frequency EPR study of the ferrous ion in the reduced rubredoxin model $[Fe(SPh)_4]^{2-}$. Inorg. Chem. 39, 281–288. [PubMed: 11272536]
43. Duboc C, Collomb MN, Pécaut J, Deronzier A, and Neese F (2008). Definition of magneto-structural correlations for the MnII ion. Chem. A Eur. J. 14, 6498–6509.
44. Azarkh M, Penkova LV, Kats SV, Varzatskii OA, Voloshin YZ, and Groenen EJJ (2014). A mononuclear Mn(II) pseudoclathrochelate complex studied by multi-frequency electron-paramagnetic-resonance spectroscopy. J. Phys. Chem. Lett 5, 886–889. [PubMed: 26274083]
45. Wood RM, Stucker DM, Jones LM, Lynch WB, Misra SK, and Freed JH (1999). An EPR study of some highly distorted tetrahedral manganese(II) complexes at high magnetic fields. Inorg. Chem. 38, 5384–5388.

46. Ding YS, Yu KX, Reta D, Ortu F, Winpenny REP, Zheng YZ, and Chilton NF (2018). Field- and temperature-dependent quantum tunnelling of the magnetisation in a large barrier single-molecule magnet. Nat. Commun. 9, 1–10. [PubMed: 29317637]
47. Cole KS, and Cole RH (1941). Dispersion and absorption in dielectrics I. Alternating current characteristics. J. Chem. Phys. 9, 341–351.
48. Orbach R (1961). Spin-lattice relaxation in rare-earth salts. Proc. R. Soc. A Math. Phys. Eng. Sci. 264, 458–484.
49. Molnár G, Mikolasek M, Ridier K, Fahs A, Nicolazzi W, and Bousseksou A (2019). Molecular spin crossover materials: review of the lattice dynamical properties. Ann. Phys. 531, 1–21.
50. Nava A, Rigamonti L, Zangrando E, Sessoli R, Wernsdorfer W, and Cornia A (2015). Redox-controlled exchange bias in a supramolecular chain of Fe4 single-molecule magnets. Angew. Chem. Int. Ed. Engl. 54, 8777–8782. [PubMed: 26096860]
51. Krylov DS, Liu F, Brandenburg A, Spree L, Bon V, Kaskel S, Wolter AUB, Büchner B, Avdoshenko SM, and Popov AA (2018). Magnetization relaxation in the single-ion magnet $DySc_2N@C_{80}$: quantum tunneling, magnetic dilution, and unconventional temperature dependence. Phys. Chem. Chem. Phys. 20, 11656–11672. [PubMed: 29671443]
52. Henderson JJ, Koo C, Feng PL, Barco E, Hill S, Tupitsyn IS, Stamp PCE, and Hendrickson DN (2009). Manifestation of spin selection rules on the quantum tunneling of magnetization in a single-molecule magnet. Phys. Rev. Lett. 103, 017202. [PubMed: 19659173]
53. Kubo R, and Toyabe T (1968). International conference on magnetic resonance and relaxation. In Magnetic resonance and relaxation: Proceedings of the XIVth Colloque Ljubljana Ampere, Blinc R, Hadzi D, and Osredkar M, eds., p. 810.
54. Kita S, Uchida K, Miyamoto R, and Iwaizumi M (1992). Spin-spin couplings in the copper acetate hydrate dimer studied by single crystal ^{13}C ENDOR for zinc-doped copper acetate monohydrate. Chem. Lett. 21, 1329–1332.
55. Paulson JA, Krost DA, McPherson GL, Rogers RD, and Atwood JL (1980). Structural, spectroscopic, and theoretical studies of an exchange-coupled manganese(II)-copper(II) dimer. Inorg. Chem. 19, 2519–2525.
56. Krost DA, and McPherson GL (1978). Spectroscopic and magnetic properties of an exchange coupled copper(II)-manganese(II) dimer. J. Am. Chem. Soc. 100, 987–989.
57. Bronova A, Kannengießer N, and Glaum R (2017). Optical spectra and magnetic behavior of a wide range of europium(III) oxo-compounds: analysis of the ligand-field effects. Inorg. Chem. 56, 9235–9246. [PubMed: 28731334]
58. Demir S, Jeon I-R, Long JR, and Harris TD (2015). Radical ligand-containing single-molecule magnets. Coord. Chem. Rev. 289–290, 149–176.
59. Gómez-Coca S, Aravena D, Morales R, and Ruiz E (2015). Large magnetic anisotropy in mononuclear metal complexes. Coord. Chem. Rev. 289–290, 379–392.
60. Jackson CE, Moseley IP, Martinez R, Sung S, and Zadrozny JM (2021). A reaction-coordinate perspective of magnetic relaxation. Chem. Soc. Rev. 50, 6684–6699. [PubMed: 33949521]
61. Murphy J (1966). Spin-Lattice relaxation due to local vibrations with temperature-independent amplitudes. Phys. Rev. 145, 241–247.
62. Goldfarb D, and Stoll S, eds. (2018). EPR Spectroscopy: Fundamentals and Methods (Wiley-VCH).

Highlights

- Integerspin, positive-D diluents are effective at slowing magnetic relaxation
- Tunneling is disrupted when dipolar field amplitudes approach zero
- There is a linear dependence of the relaxation rate on dilution level

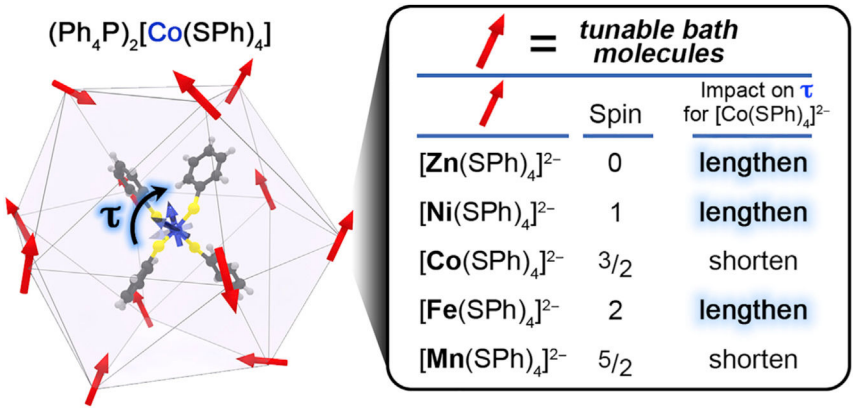

Figure 1. Summary of present work

(Left) The local environment of $[Co(SPh)_4]^{2-}$ in crystals of pure $(Ph_4P)_2[Co(SPh)_4]$ (Co) is rich in high-spin Co(II) ions. (Right) We show via chemical control of the spin bath that certain paramagnetic diluents can lengthen magnetic relaxation times (τ) analogous to diamagnetic diluents, like Zn^{2+}.

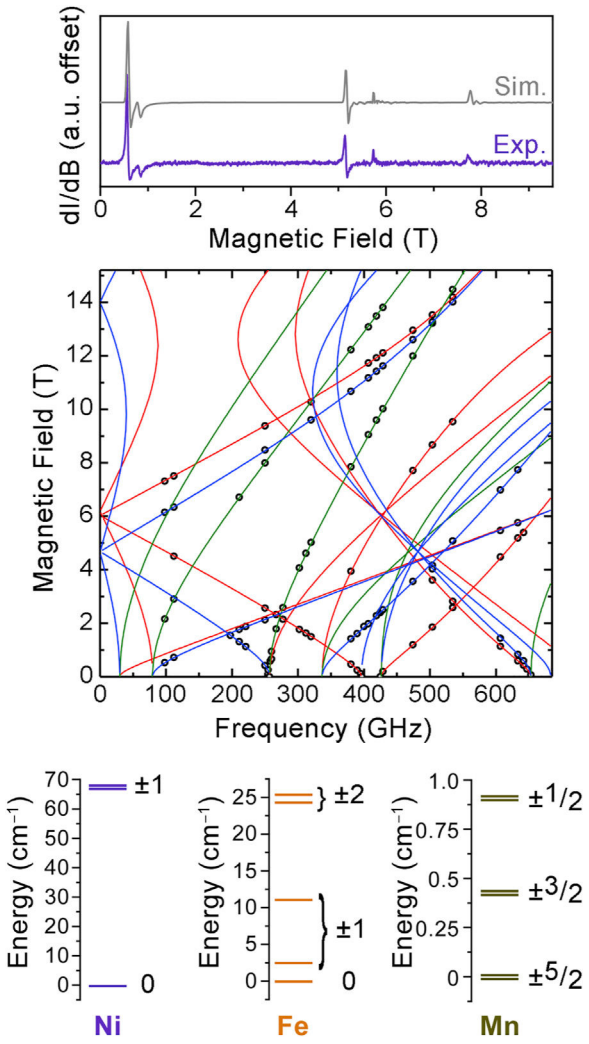

Figure 2. HFHF-EPR data summary

(Top) The 633-GHz EPR spectra for a powder of Fe collected at 20 K. See supplemental information for experimental and simulation details. (Middle) Field versus frequency dependence of the EPR transitions for Fe. Each circle represents a transition observed at that field and frequency. Green, blue, and red lines were calculated with the Fe x, y, and z axes, respectively, aligned with the magnetic field. (Bottom) Zero-field energies of the M_S levels for Ni, Fe, and Mn calculated using the spin Hamiltonian parameters derived from EPR and dc susceptibility analyses. Note that M_S labels for Fe correspond to high-field values; near zero-field, the $M_S = \pm 1$ levels are highly mixed by E, and for Mn, the energies of the Kramers doublets (e.g., the $\pm 5/2$ M_S levels) are actually degenerate but depicted as separate for clarity. Levels for Mn are depicted assuming $D < 0$.

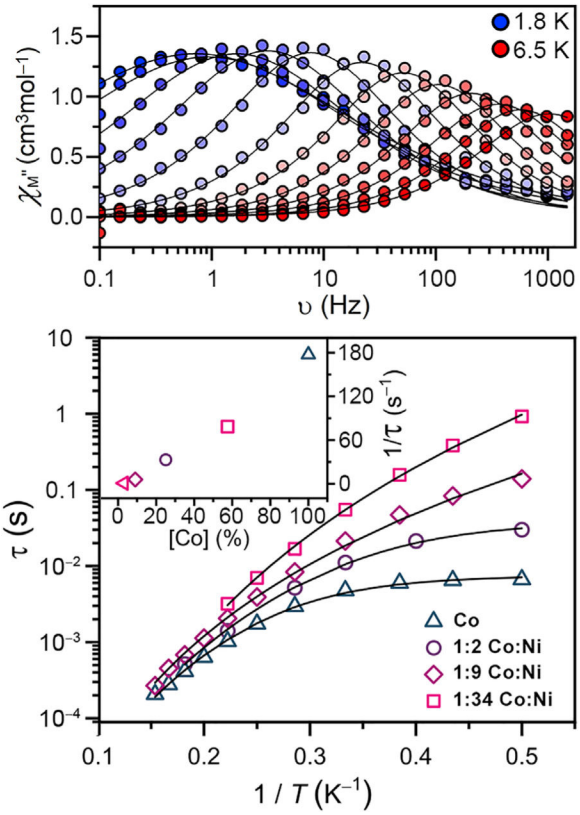

Figure 3. Ac susceptibility and extracted relaxation times

(Top) Out-of-phase ac susceptibility data (χ_M'') for a 1:9 dilution of Co in Ni as a function of temperature in zero applied magnetic field. Data were collected at temperature intervals of 0.3 K from 1.8 K to 2.7 K and intervals of 0.5 K from 3.0 to 6.5 K. Lines were generated via fits to the Cole-Cole equation (see supplemental information). (Bottom) Temperature dependence of the zero-field relaxation times (τ) for Co dilutions in Ni. Solid black lines are fits of the temperature dependence following the Raman and tunneling model proposed in the main text. Inset: $1/\tau$ (at 2.0 K) as a function of dilution level.

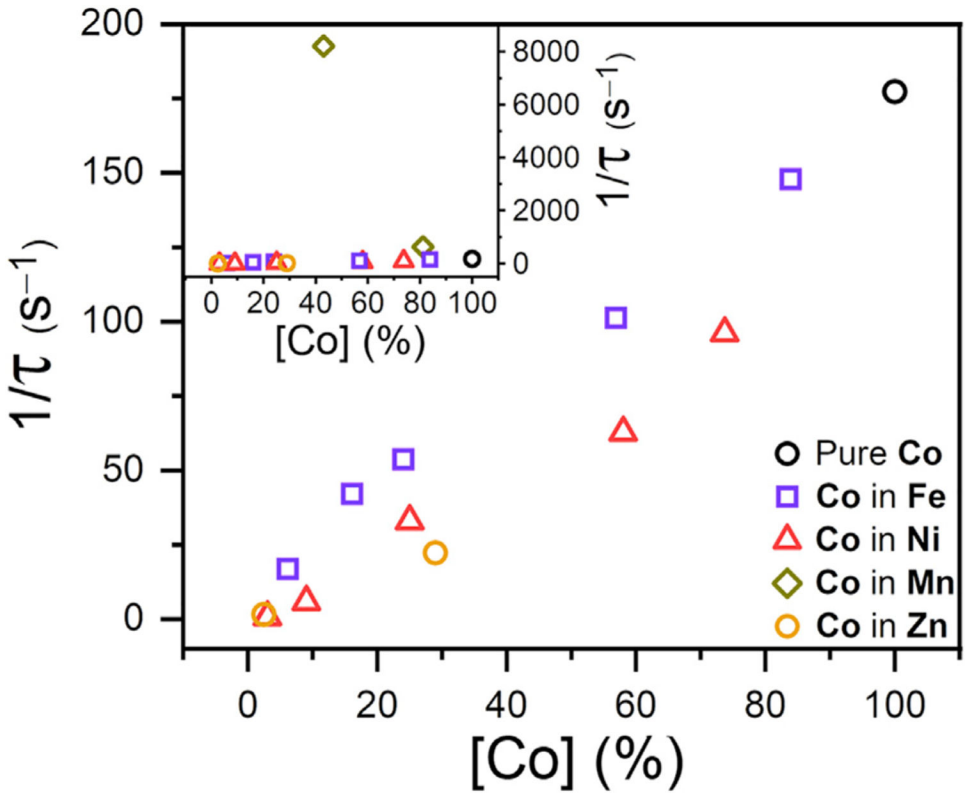

Figure 4. Dilution-dependent relaxation rates

Variable-concentration relaxation rates (1/**τ**) for Co diluted in Ni, Fe, Mn, and Zn. All relaxation rates were extracted from variable-frequency ac susceptibility measurements at 2 K and zero applied magnetic field. Inset: scale altered to show Mn dilution data.

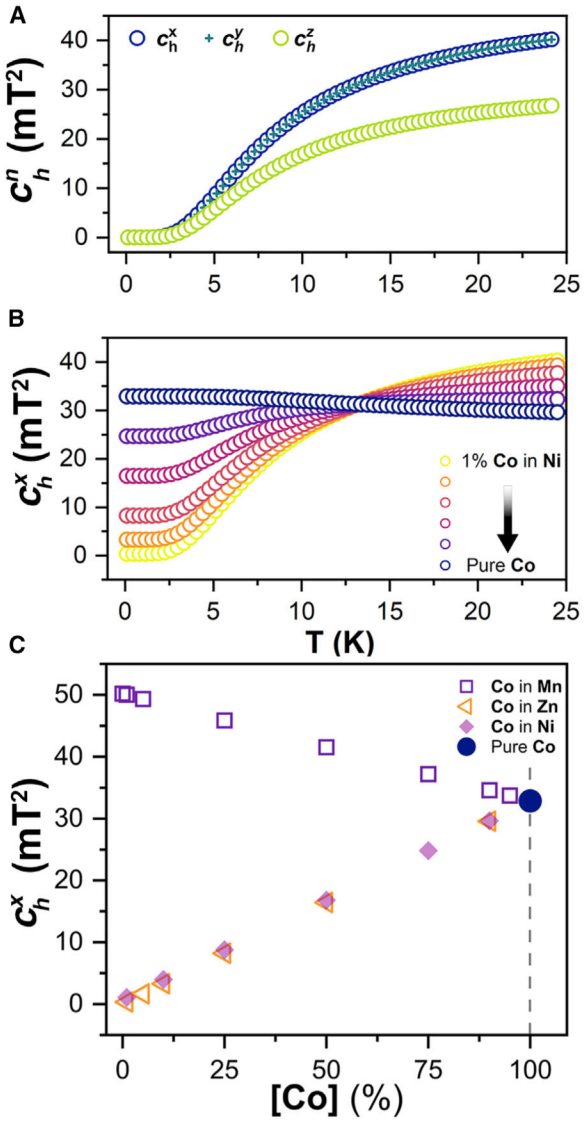

Figure 5. Dipolar field calculations

(A) Computed variable-temperature local dipolar field variance for the *x*, *y*, and *z* components $\left(c_h^{x,\,y,\,z}\right)$ of pure Ni.

(B) Computed variable-temperature c_h^x for a $[Co(SPh)_4]^{2-}$ embedded in Ni.

(C) Computed variable-concentration c_h^x for $[Co(SPh)_4]^{2-}$ diluted in Mn, Ni, and Zn at 2.6 K.